Preprint Title Facile preparation and photocatalytic performance of anatase TiO_2/nanocellulose composite

Authors Guoqing Liu, Xiangjun Pan, Jing Li, Cheng Li and Chenlu Ji

Publication Date 13 Aug. 2021

Article Type Full Research Paper

ORCID® iDs Guoqing Liu - https://orcid.org/0000-0001-8260-7495

Facile preparation and photocatalytic performance of anatase TiO_2/nanocellulose composite

Guoqing Liu*[1], Xiangjun Pan[1], Jing Li[2], Cheng Li[1] and Chenlu Ji[1]

Address: [1]College of Chemical and Material Engineering, Quzhou University, Quzhou, Zhejiang 324000, China and [2]College of Chemical and Biological Engineering, Zhejiang University, Hangzhou, Zhejiang 310027, China

Email: Guoqing Liu* - liuguoqingmr@126.com

* Corresponding author

Abstract

Anatase TiO_2/nanocellulose composite was prepared for the first time via a one-step method at a relatively low temperature by using cellulose nanofibers as carrier and tetrabutyl titanate as titanium precursor. The morphology, structure and element composition of the composite were characterized by SEM, EDS, TEM, XRD and XPS. The specific surface area and thermal stability of the composite were investigated by N_2 adsorption-desorption and thermogravimetric analysis, respectively. In addition, the prepared composite was used for the photocatalytic degradation of methyl orange (aqueous solution, 40 mg·L^{-1}). It was found that the composite had a good morphology and anatase crystal structure, and Ti-O-C bond was formed between TiO_2 and nanocellulose. The specific surface area of composite was increased and the thermal stability was decreased compared with the cellulose nanofiber. Moreover, the degradation rate of methyl orange was achieved as 99.72% within 30 min, and no

obvious activity loss was observed after five cycles. This work might give some insights into the design of efficient photocatalysts for the treatment of organic dye wastewater.

Keywords

cellulose nanofiber; anatase; TiO_2; photocatalytic degradation efficiency

Introduction

Organic dyes are widely used in textile, paper and dye industries. However, wastewater produced by this process is toxic and difficult to degrade, which is harmful to humans' health and the environment. Therefore, it is highly urgent to explore effective methods for the degradation of organic dye wastewater. At present, the methods for treating organic dye wastewater mainly include physical adsorption, membrane filtration, ion exchange, chemical oxidation, biochemistry, etc. [1-6], but these methods have some disadvantages (such as incomplete degradation of pollutants and secondary pollution). In this regard, photocatalytic degradation is considered as one of the most effective methods for the treatment of organic dye wastewater due to its advantages such as simplicity, high efficiency, and environmentally-friendly characteristic [7-10], and the organic dyes can be degraded into non-toxic and harmless molecules (such as CO_2 and H_2O) under light conditions by using photocatalysts [10-12].

As a semiconductor, nano TiO_2 has been widely used in the field of photocatalytic degradation owing to the advantages (such as good stability and non-toxicity) [13-14]. As for TiO_2, there are mainly three crystal structures: rutile, anatase and brookite. Among them, anatase has better photocatalytic activity and is most widely used in practical applications due to its wider band gap [15]. However, TiO_2 nanoparticle tends

to agglomerate inevitably in practical photocatalytic applications and it is also difficult to recycle. Therefore, in recent years, researchers have reported the strategy by supporting nanoparticles on various carriers (such as glass, stainless steel [16-18], cellulose [19-25]) to overcome the above problem, meanwhile, the construction of TiO_2-based composite would be beneficial to achieve better photocatalytic performance.

As the most abundant natural biomass resource, cellulose has the advantages of non-toxic, environmentally friendly, and renewable. Therefore, the preparation of nano TiO_2 composite with cellulose as a carrier has become a research hotspot in this field. According to the reports, there are mainly four preparation methods: 1) TiO_2 gel film/cellulose composite material was prepared via a sol-gel method and then it was calcined to obtain anatase TiO_2/nanocellulose composite [19-20]; 2) TiO_2 gel film/cellulose composite was first prepared by sol-gel method with multilayer deposition, and then followed by hydrothermal treatment to get the anatase TiO_2/cellulose composite [21]. 3) Nanocellulose aerogel was prepared before tetrabutyl titanate adsorbed, and followed by hydrothermal treatment to get the TiO_2/nanocellulose composite [22]. 4) Nano TiO_2 was first prepared, and then it was mixed with nanocellulose solution to prepare the TiO_2/nanocellulose composite [23-24]. However, the above methods included multi-step synthesis and the preparation process was relatively complicated, and the conversion of amorphous or rutile TiO_2 into anatase TiO_2 usually required high temperature. In this regard, this work reported the one-step method to synthesize anatase TiO_2/cellulose composites at a lower temperature by using flexible cellulose nanofibers as a carrier. Tetrabutyl titanate was used as titanium precursor, ethanol and water was used as solvent, and the mixture was stirred for 5 h at 55 °C, and followed by aging, washing and freeze-drying to get the anatase TiO_2/nanocellulose composite, and it was found that the prepared composite exhibited excellent performance for the degradation of methyl orange.

Results and Discussion

SEM and EDS analysis

The surface morphology and element composition of the sample was investigated by scanning electron microscope equipped with an energy spectrum detector, and the results were shown in Figure 1. It could be seen from Figure 1a that three-dimensional network structure of cellulose interwoven by fine nanofibrils still remained, and numerous nanopores on the surface were also observed. In addition, it was found that a large number of TiO_2 nanoparticles were supported uniformly on nanocellulose. Figure 1b shows the energy dispersive X-ray spectroscopy (EDS) result of the sample, besides the two characteristic peaks of C and O, the strong characteristic peaks of Ti was also found. The atomic percentages of C, O, and Ti were 40.5, 51.9, and 7.6%, respectively. The C/O atomic ratio of TiO_2/CNF composite was 0.78, which was much lower than that of nanocellulose (1.2). This result further indicated that the TiO_2 nanoparticles was successfully loaded on nanocellulose, and the composite was mainly composed of three elements of C, O and Ti.

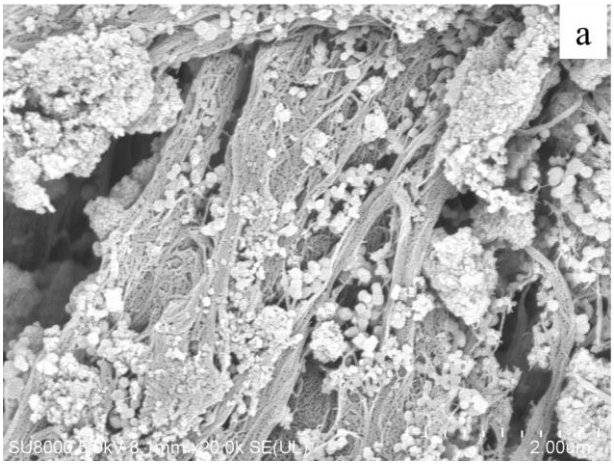

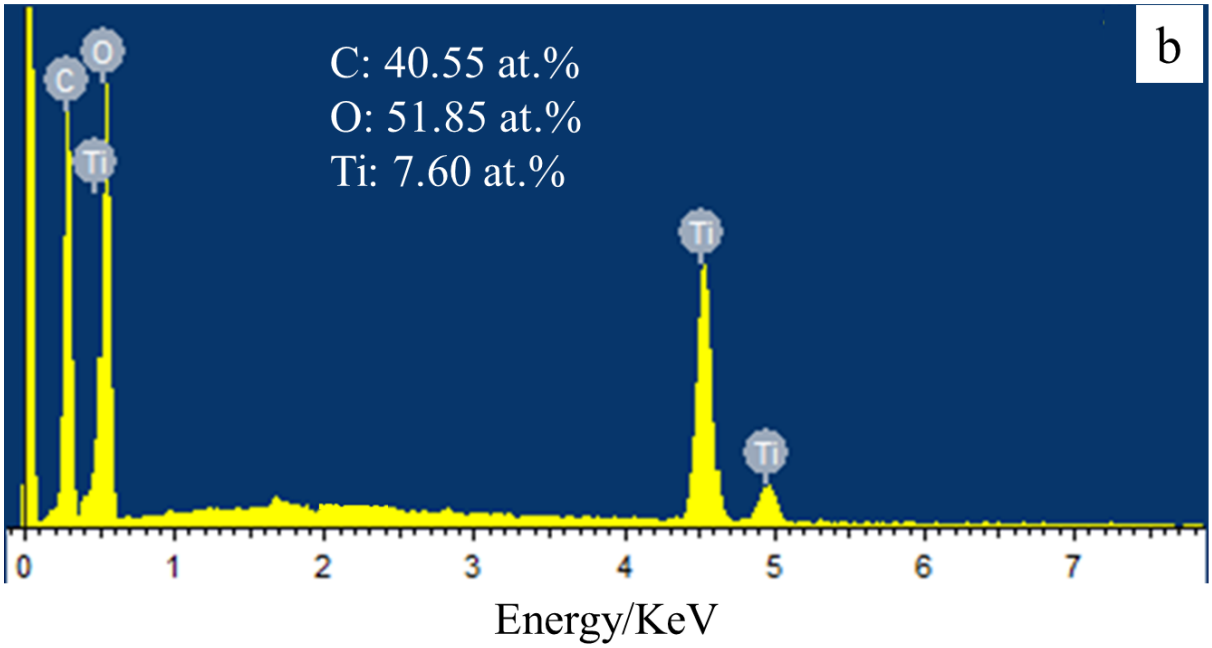

Figure 1. (a) SEM and (b) EDS images of TiO_2/CNF composite.

TEM analysis

The microstructure of the sample was further investigated by transmission electron microscope (TEM). It could be found from Figure 2a that the diameter of the nano TiO_2 nanoparticles was about 30 nm with relatively uniform size, and the particles agglomerated to form an irregular nanoporous structure. In Figure 2b, a lattice fringe with an interplanar spacing of 0.353 nm was obviously observed, which was assigned to (101) plane of anatase TiO_2 [25]. In addition, this result also indicated that the prepared TiO_2 had good crystallinity.

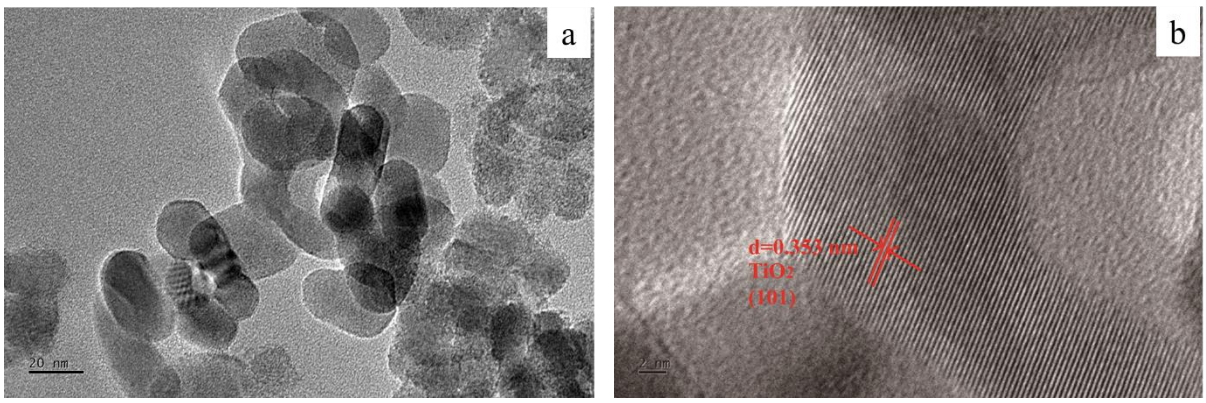

Figure 2. (a) TEM and (b) HRTEM images of TiO_2/CNF composite.

XRD analysis

XRD was used to characterize the crystal structure of the prepared composite, and the results were shown in Figure 3. The characteristic XRD diffraction peaks at 2θ = 15.16, 16.82, 22.82 and 34.94° of cellulose I were observed, which were assigned to (101), (10-1), (002) and (040) planes, respectively. As for TiO_2/CNF composite, other XRD patterns at 2θ = 25.66, 38.04, 48.30, 54.18, 55.14, 62.98, 68.80, 70.46 and 75.31° were attributed to (101), (004), (200), (105), (211), (204), (116), (220) and (215) planes of anatase TiO_2 [23], and no characteristic peaks of rutile and brookite TiO_2 were found. This result indicated that the anatase TiO_2/CNF with high purity and good crystallinity was successfully prepared.

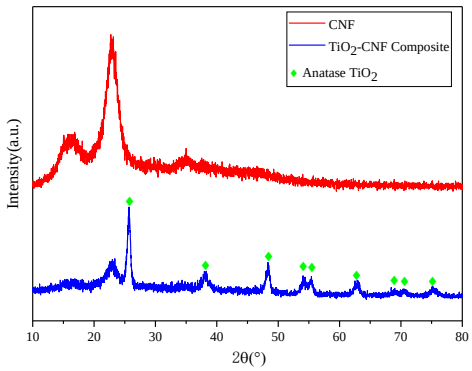

Figure 3. XRD patterns of CNF and TiO_2/CNF composite.

XPS analysis

X-ray photoelectron spectroscopy (XPS) was used to characterize the elemental composition of the prepared samples (as shown in Figure 4). The characteristic peaks at binding energies of 285 and 534 eV in Figure 4a were assigned to C1s and O1s, respectively. The characteristic peak at binding energy of 459 eV in Figure 4b was assigned to Ti 2p, the result indicated that the existence of elements C、O and Ti among the composite. The atomic percentages of C, O and Ti are 42.16, 50.98 and 6.86%, respectively, consistent with the EDS result. The characteristic peaks at 458.58

and 464.38 eV in Figure 4c were ascribed to Ti $2p_{3/2}$ and Ti $2p_{1/2}$, respectively, indicating that the existence of Ti^{4+} among the composite [26]. Compared to that of the bare TiO_2, the binding energy of Ti 2p of the composite shifted to higher position, indicating that the electronic environment of Ti had changed due to the existence of Ti-O-C bond [27]. Such a shift of binding energy showed that TiO_2 was loaded on nanocellulose by chemical bonds with a strong chemical effect. Figure 4d shows the high-resolution O1s XPS spectrum of TiO_2/CNF, and the characteristic peaks at 529.93 and 532.48 eV were ascribed to Ti-O and O-H bonds, respectively. The above results showed that the TiO_2/nanocellulose composite with strong chemical interaction was successfully prepared.

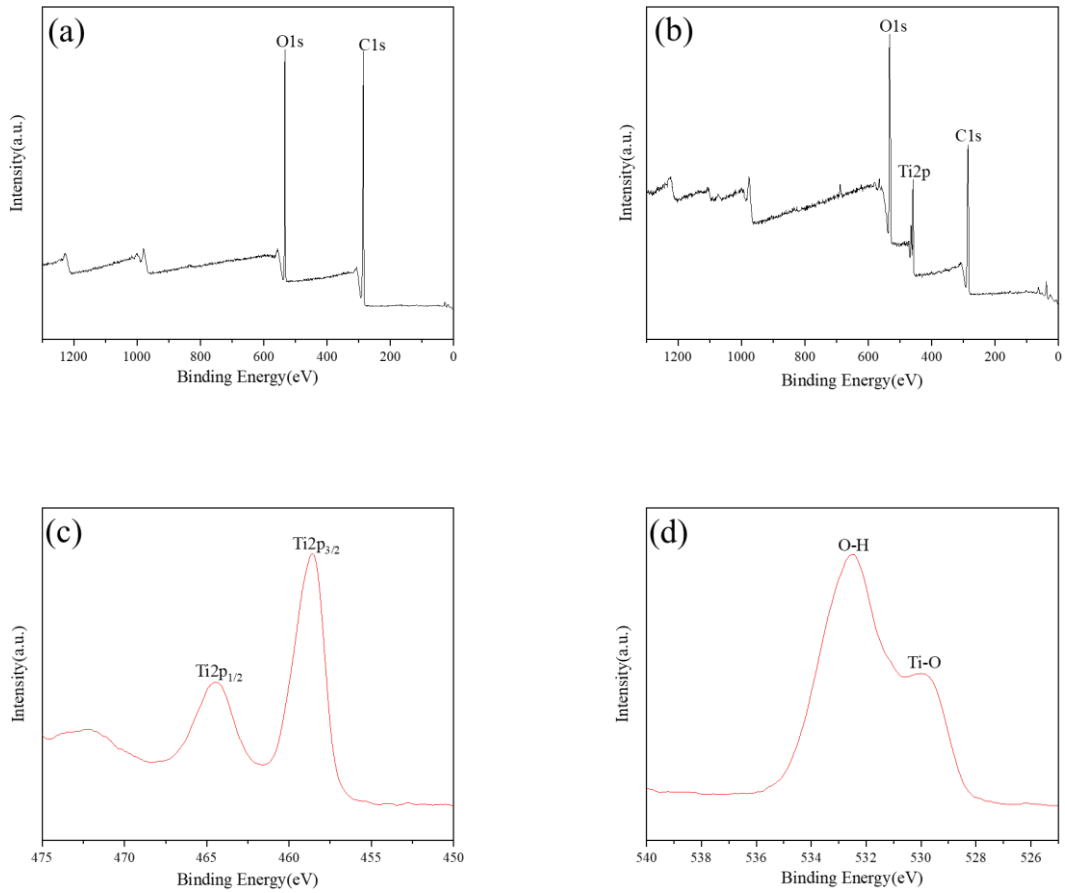

Figure 4. XPS survey of (a) CNF and (b) TiO_2/CNF, high-resolution XPS spectra of (c) Ti 2p and (d) O 1s of TiO_2/CNF.

N_2 adsorption-desorption analysis

The specific surface area, pore specific surface area, pore volume and pore diameter of CNF and TiO_2/CNF were measured by N_2 adsorption-desorption, and the results were shown in Table 1. It can be seen that the specific surface area and pore volume of the TiO_2-CNF composite were 54.2 $m^2 \cdot g^{-1}$ and 0.0253 $cm^3 \cdot g^{-1}$, respectively, which were significantly increased compared to those of CNF. The pore specific surface area was 50.099 $m^2 \cdot g^{-1}$, which accounted for up to 92.46% of the total specific surface area. That was due to the fact that tetrabutyl titanate had penetrated into the voids of the nanocellulose during the preparation process and chemically interacted with its hydroxyl groups, which destroyed the cross-linked structure of CNF and promoted the formation of mesopores. On the other hand, the formation of nano TiO_2 promoted the formation of three-dimensional structures inside and on the surface of the composite. However, the pore size of TiO_2/CNF did not change significantly compared to that of CNF, and the pore specific surface area ratio was very high, indicating that the generated TiO_2 particles might have a large number of small nanopores.

Table 1: The structural properties of the prepared samples

Sample	S_{BET} /$m^2 \cdot g^{-1}$	Pore SSA /$m^2 \cdot g^{-1}$	Pore volume /$cm^3 \cdot g^{-1}$	Pore diameter /nm
CNF	2.4	1.371	0.0007	1.0115
TiO_2-CNF	54.2	50.099	0.0253	1.0934

Thermogravimetric analysis

Thermogravimetric analysis was used to characterize the thermal stability of CNF and TiO_2/CNF. It was seen from Figure 5 that the thermal decomposition process of CNF and TiO_2/CNF was divided into three stages: initial thermal decomposition, rapid thermal decomposition and slow thermal decomposition. The initial decomposition

temperatures of CNF and TiO_2/CNF were 277 and 223 °C, respectively. The DTG curves showed that CNF and TiO_2/CNF had characteristic peaks at 352 and 302 °C, respectively, which was the maximum weight loss rate temperature of the sample. After reaching 400 °C, the thermal degradation rates of CNF and TiO_2/CNF both decreased significantly, and underwent a slow thermal decomposition process. It should be noted that the initial decomposition temperature and maximum weight loss rate temperature of TiO_2/CNF were both lowered by more than 50 °C compared to those of CNF, indicating that the thermal stability of TiO_2/CNF had been significantly reduced. That was mainly due to the TiO_2 had reacted chemically with the hydroxy group on the surface of nanocellulose. In addition, a small amount of nitric acid solution was added during the preparation process, leading to the destruction of the cross-linked structure and crystal structure of CNF, which was consistent with the weakening characteristic XRD peaks of nanocellulose. When the thermal decomposition temperature was close to 500 °C, the residual rates of CNF and TiO_2/CNF were 20.75 and 38.28%, respectively, and the loading content of TiO_2 was calculated to be 17.53% among the TiO_2/CNF composite.

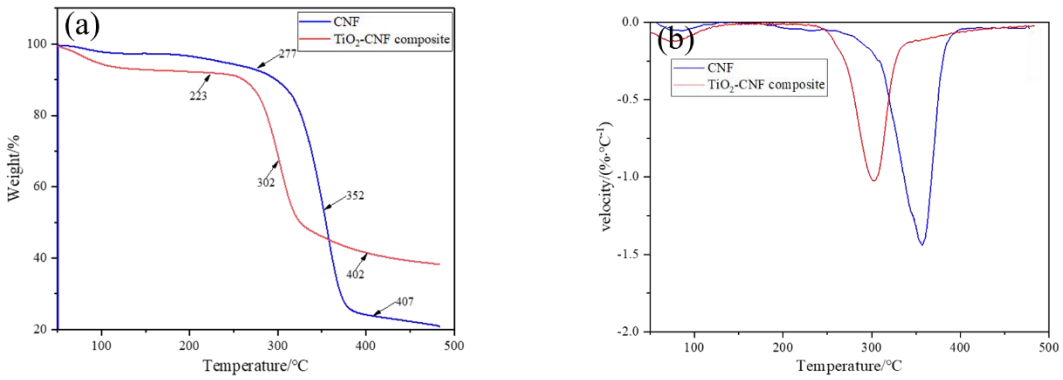

Figure 5. (a) TG curves of CNF and TiO_2/CNF, (b) DTG curves of CNF and TiO_2/CNF.

Photocatalytic activity test

The photocatalytic degradation performance of bare TiO_2, CNF and TiO_2/CNF on methyl orange was investigated, and the results were shown in Figure 6. It was found that the photocatalytic degradation rates of bare TiO_2 and TiO_2/CNF to methyl orange increased with the extension of UV irradiation time. Compared to that of bare TiO_2, the photocatalytic degradation rate of TiO_2/CNF was much higher, and the bare CNF basically showed no photocatalytic degradation performance. When UV light was irradiated for 30 min, the degradation rates of bare TiO_2 and TiO_2/CNF to methyl orange were 69.18 and 99.72%, respectively. The photocatalytic performance of TiO_2/CNF composite was significantly improved compared to that of bare TiO_2, and methyl orange was completely degraded within 30 min. That was mainly because the combination of CNF promoted the rapid transfer of electrons generated by TiO_2 under light conditions to CNF through the Ti-O-C bond among the composite, which effectively reduced the recombination rate of photogenerated electrons and holes, thereby enhancing the photocatalytic performance of TiO_2/CNF composite.

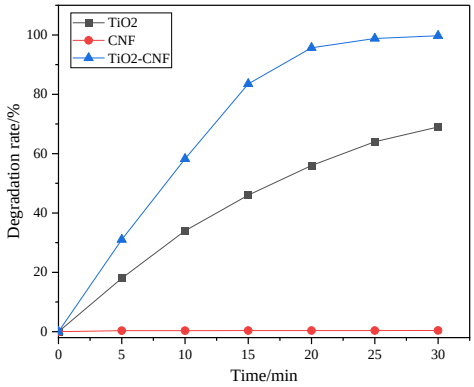

Figure 6. Photocatalytic degradation rate of methyl orange over TiO_2、CNF and TiO_2/CNF.

In order to investigate the photocatalytic stability of TiO_2/CNF, the sample after photocatalytic degradation of methyl orange was recovered for five cycles, the

degradation rate was tested, and the results were shown in Figure 7. It was found that as the number of cycles increased, the degradation rate decreased slightly. After five cycles, the degradation rate of the composite to methyl orange was still as high as 98.39%, no obvious loss in catalytic activity was observed, displaying excellent photocatalytic stability. The result showed that the TiO_2 was supported on nanocellulose strongly to form the TiO_2/CNF composite, and because of the good loading performance, CNF still provided a transfer environment for the photogenerated electrons of TiO_2, further reduced the photo-corrosion of TiO_2 and ensured its good photocatalytic stability.

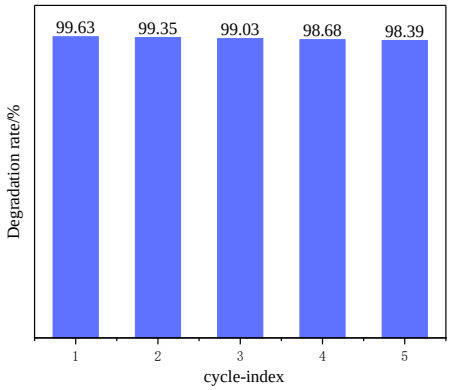

Figure 7. Photocatalytic degradation rate of TiO_2/CNF on methyl orange after five cycle under light for 30 min.

Conclusion

(1) The results of SEM, EDS, TEM, XRD and XPS showed that the anatase TiO_2/nanocellulose composite with good crystallinity was successfully prepared by one-step method at low temperature. The degradation rate of methyl orange solution was as high as 99.72%, displaying fast and efficient photocatalytic performance.

(2) BET and TG results indicated that the combination of nanocellulose significantly increased the specific surface area and pore volume of TiO_2/CNF composite, but the thermal stability was reduced, and the loading mass content of TiO_2 was about 17.53%.

(3) TiO_2/nanocellulose composite showed good recycling performance. After five cycles, the degradation rate of methyl orange was only slightly reduced, still as high as 98.39%. The prepared TiO_2/CNF composite was a promising candidate for the degradation of organic dye wastewater.

Experimental

Instruments and reagents

Experimental instrument: centrifuge (TDL-60B, Shanghai Anting scientific instrument factory), freeze dryer (LC-10N-50A, Zhejiang Lichen instrument technology Co., Ltd.), photochemical reactor (YZ-GHX-A, Yanzheng instrument company), UV-visible spectrophotometer (752N, Shanghai INESA instrument Co., Ltd.), X-ray diffractometer (XRD-6100, Shimadzu corporation); X-ray photoelectron spectrometer (K-Alpha, Thermo Fisher technology Co., Ltd.), field emission scanning electron microscope (equipped with energy spectrum detector, SU8010, Hitachi Co., Ltd.), transmission electron microscope (JEM-2100, Japan electronics corporation), automatic rapid surface and porosity analyzer (Gemini VII 2390, Micromeritics

instrument Co., USA), thermogravimetric analyzer (TGA2, Mettler Toledo, Switzerland).

Reagent: tetrabutyl titanate (99%) was provided by Shanghai Titan technology Co., Ltd.; nanocellulose (1wt%) was provided by Jinjiahao green nanomaterials Co., Ltd.; ethanol (AR, ≥99.7%) was provided by Ante food Co., Ltd.; nitric acid (AR, 65-68%) was provided by Xilong scientific; methyl orange was provided by Shanghai Titan scientific Co., Ltd.

Preparation of anatase TiO_2/nanocellulose composite (TiO_2/CNF)

1 mL of tetrabutyl titanate and 5 mL of ethanol were mixed and then stirred vigorously, and the solution was denoted as A. 40 g of 1wt% CNF emulsion was diluted to 0.5wt % with a mixed solvent of ethanol and water (1:1) under continuous stirring, and nitric acid solution was added until the pH value was around 2, and the solution was denoted as B. Afterwards, solution A was added into solution B dropwise, and the mixture was reacted for 5 h at 55 °C. After the reaction, the mixture underwent an aging process for 24 h. The solid sample was obtained by filtration, and followed by washing with water and ethanol thoroughly until the pH value of the filtrate was neutral. Finally, the resultant sample was freeze-dried for 48 h to obtain the anatase TiO_2/nanocellulose composite (TiO_2/CNF).

Photocatalytic activity test

In order to study the photocatalytic performance of anatase TiO_2/nanocellulose composite, a photocatalytic experiment was carried out with methyl orange as the target degradation product, and the degradation rate under ultraviolet light was investigated. 20 mg of the sample was added into a tube containing 20 mL of methyl orange solution (40 mg/L), and the tube was placed in the photoreactor and stirred for

30 min in the dark to achieve the equilibrium of the solution absorption and desorption. Then the photocatalytic reaction was started with the light turned on. The power of the ultraviolet lamp was 500 W and the wavelength was 365 nm. The supernatant in the tube was analyzed by ultraviolet-visible spectrophotometer at 463 nm. The degradation rate (ηt) at the photodegradation time (t) was calculated: $\eta t=[(A_0-A_t)/A_0]\times100\%$, where A_0 was the initial absorbance of solution, and A_t was the absorbance of the solution at the time of t.

Bare TiO_2 was also prepared via the above method for the purpose of comparison. In order to investigate the photocatalytic degradation stability, the sample after the photocatalytic reaction was centrifuged and the supernatant was removed. 20 mL of methyl orange solution (40 mg/L) was added again, and then the photocatalytic reaction was carried out for 30 min under the same light conditions. The degradation rate was determined, and it was repeated five times to investigate the change of its photocatalytic degradation performance.

Funding

This work was supported by Basic Public Welfare Research Project of Zhejiang Province (LGG21B060001), and Science and Technology Project of Institute of Zhejiang University-Quzhou (IZQ2019-KJ-026).

References

1. Dong L. L. Environmental Science Survey, 2002, 21, 49-51. doi:10.3969/j.issn.1673-9655.2002.03.015
2. Ergene A.; Ada K.; Tan S.; Katırcıoğlu H. Desalination, 2009, 249, 1308-1314. doi:10.1016/j.desal.2009.06.027

3. Wang S. W.; Chen S.; Sun D. Z. Industrial Water Treatment, 2010, 30, 8-12. doi:10.1017/S0022381609990582
4. Jadhav A. J.; Srivastava V. C. Chem. Eng. J. 2013, 229, 450-459. doi:10.1016/j.cej.2013.06.021
5. Yu H. G.; Xiao P.; Tian J.; Wang F. Z.; Yu J. G. ACS Appl. Mater. Inter. 2016,8,29470-29477. doi:10.1021/acsami.6b09903
6. Feng J.; Darren M. D.; Hsieh Y. L. Carbohyd. Polym. 2017, 173, 286-294. doi:10.1016/j.carbpol.2017.05.097
7. Chen X. B.; Liu L.; Yu P. Y.; Mao S. S. Science. 2011, 331, 746-750. doi:10.1126/science.1200448
8. Xu Y.; Mo Y. P.; Tian J.; Wang P.; Yu H. G.; Yu J. G. Appl. Catal. B-Environ. 2016, 181, 810-817. doi:10.1016/j.apcatb.2015.08.049
9. Ali A. I.; Amir P.; Moslem F.; Sahand J.; Babak K. Appl. Surf. Sci. 2018, 462, 549-564. doi:10.1016/j.apsusc.2018.08.133
10. Hoffmann M. R.; Martin S. T.; Choi W.; Bahnemann D. W. Chem. Rev. 1995, 95, 69-96. doi:10.1021/cr00033a004
11. Wang P.; Wang J.; Wang X.; Yu H.; Yu J.; Lei M.; Wang Y. Appl. Catal. B-Environ. 2013, 132-133, 452-459. doi:10.1016/j.apcatb.2012.12.009
12. Tian F.; Wu Z.; Chen Q.; Yan Y.; Cravotto G.; Wu Z. Appl. Surf. Sci. 2015, 351, 104-112. doi: 10.1016/j.apsusc.2015.05.133
13. Linsebigler A. L.; Lu G.; Yates J. T. Chem. Rev. 1995, 95, 735–758. doi: 10.1021/cr00035a013
14. Tong H.; Ouyang S.; Bi Y.; Umezawa N.; Oshikiri M.; Ye J. Adv. Mater. 2012, 24, 229-251. doi:10.1002/chin.201210222
15. Pan L.; Huang H.; Lim C. K.; Hong Q. Y.; Tse M. S.; Tan O. K. RSC Adv. 2013, 3, 3566-3571. doi:10.1039/c3ra22842h

16. Fernández A.; Lassaletta G.; Jiménez V. M.; Justo A.; González-Elipe A. R.; Herr mann J. M.; Tahiri H.; Ait-Ichou Y. Appl. Catal. B-Environ. 1995, 7, 49-63. doi:10. 1016/0926-3373(95)00026-7
17. O'Neill S. A.; Clark R. J. H.; Parkin I. P.; Elliott N.; Mills A. Chem. Mater. 2003, 15 , 46-50. doi:10.1021/cm020707f
18. Philip E.; Martyn E. P.; David W. S. Chem. Mater. 2006, 18, 5750-5755. doi:10.10 21/cm060816k・・
19. Ivanova A.; Fattakhova-Rohlfing D.; Kayaalp B. E.; Rathousky J.; Bein T. J. Am. Chem. Soc. 2014, 136, 5930-5937. doi:10.1021/ja411292u
20. Huang J. G.; Kunitake T. J. Am. Chem. Soc. 2003, 125, 11834-11835. doi: 10.10 21/ja037419k
21. Yan L.; Xu J. B.; Huang J. G. CrystEngComm, 2014, 16, 464-471. doi:10.1039/c3 ce41906a
22. Liu H. L.; Peng J. J.; Li M.; Yang F. Acta Materiae Compositae Sinica, 2013, 30, 1 63-169. doi:10.13801/j.cnki.fhclxb.2013.04.001
23. An X. Y.; Wen Y. B.; Almujil A.; Cheng D.; Li J. G.; Jia X.; Zou J. J.; Ni Y. H. R SC Adv. 2016, 6, 89457–89466. doi:10.1039/C6RA21042B
24. Mohamed M. A.; Salleh W. N. W.; Jaafar J.; Ismail A. F.; Mutalib M. A.; Jamil S. M . Carbohyd. Polym. 2015, 133, 429-437. doi:10.1016/j.carbpol.2015.07.057
25. Xiong Z.; Dou H.; Pan J.; Ma J.; Xu C.; Zhao X. S. CrystEngComm, 2010, 12, 345 5-3457. doi:10.1039/c0ce00228c
26. Gu J. F.; Wen M.; Liu G.; Lv J. Rare Metal Materials and Engineering, 2011, 40, 5 23-525. doi:CNKI:SUN:COSE.0.2011-03-033
27. Qiu B.; Zhou Y.; Ma Y.; Yang X.; Sheng W.; Xing M.; Zhang J. Sci. Rep. 2015, 5, 8591-8598. doi:10.1038/srep08591